Electronic Supplementary Material (ESI) for Inorganic Chemistry Frontiers.

Supporting Information

Photoinduced Radicals Modulated NIR Photothermal Conversion in a Photochromic Inorganic-Organic Complex

Zhe Wang, [a] Tieqiang Wang, [a] Junbiao Wu, * [a] Zhuopeng Wang, [a] Jiyang Li, * [b]

a. *Department of Chemistry, College of Sciences, Northeastern University, Shenyang, Liaoning 110819, China. Email: wujunbiao@mail.neu.edu.cn;*

b. *State Key Laboratory of Inorganic Synthesis and Preparative Chemistry, College of Chemistry, Jilin University, Changchun 130012, P. R. China. E-mail: lijiyang@jlu.edu.cn*

Index

1. Supplementary Figures

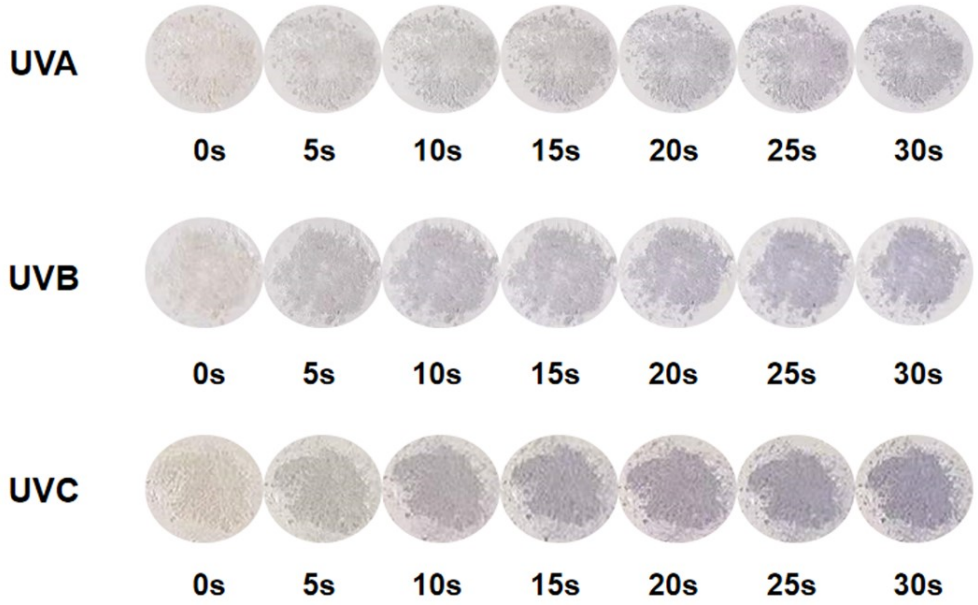

Fig. S1 Photochromic behavior of **NEU20** by different modes of UV light (UVA, UVB and UVC) irradiation.

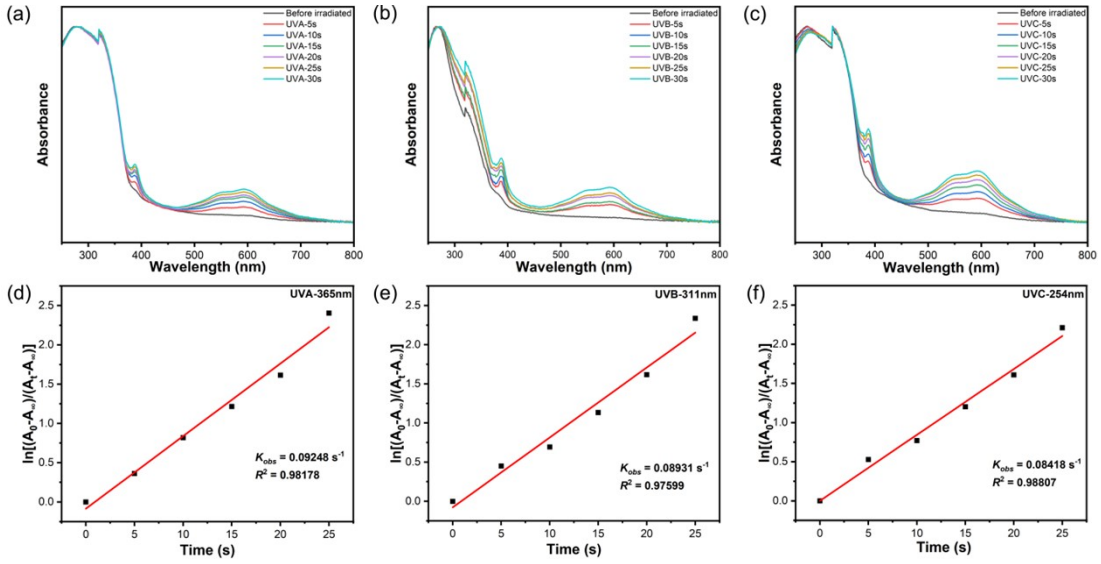

Fig. S2 *In situ* time dependent UV-Vis spectra of **NEU20** by different modes of UV light irradiation; (a) UVA light irradiation. (b) UVB light irradiation. (c) UVC light irradiation. First-order kinetic plot for change in absorbance at λ = 387 nm by different modes of UV light irradiation, where A_0, A_t, and A_∞ are the absorbance values at time zero, time *t*, and infinite time of the reaction, respectively; (d) UVA light irradiation. (e) UVB light irradiation. (f) UVC light irradiation.

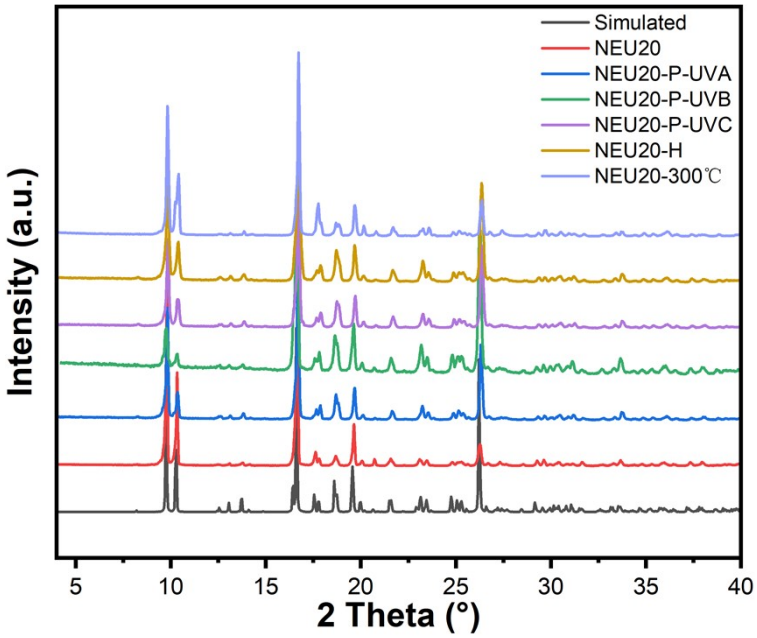

Fig. S3 PXRD for **NEU20** and other samples that obtained by different modes.

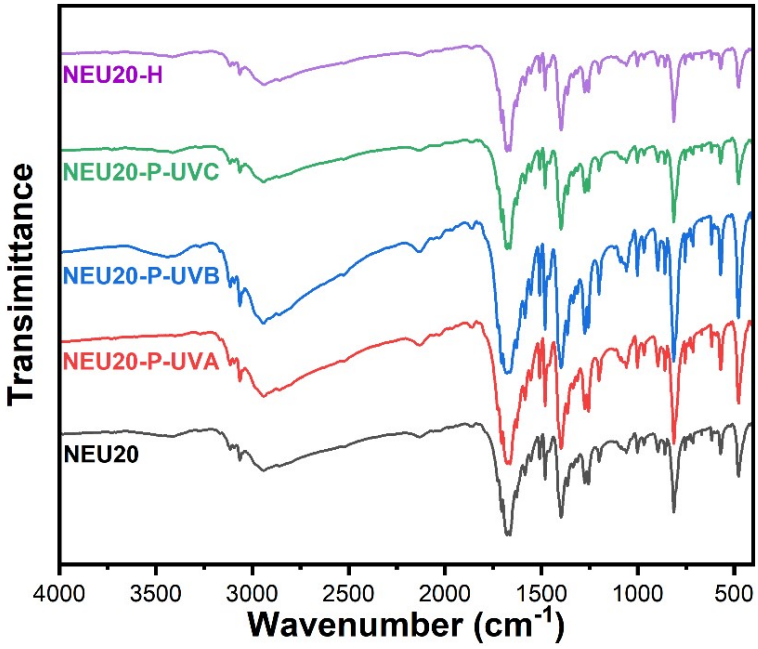

Fig. S4 IR spectra for **NEU20** and other samples that obtained by different modes.

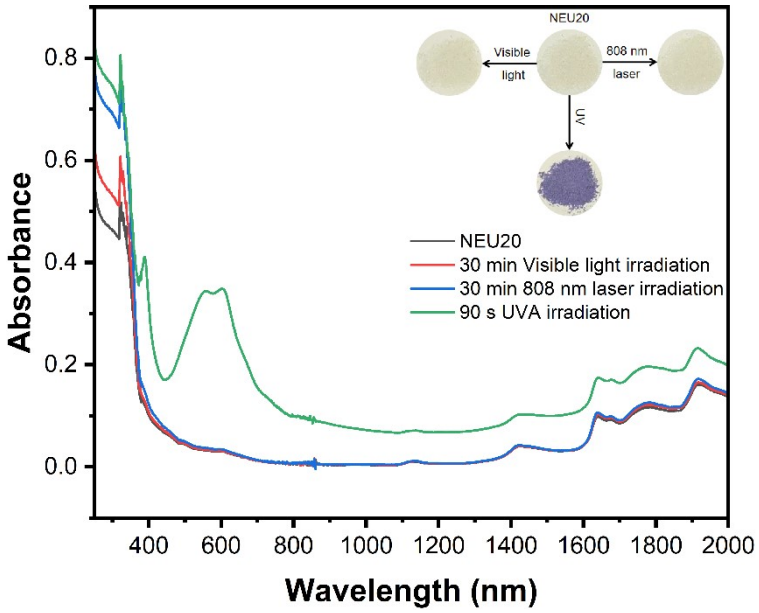

Fig. S5 UV-Vis-IR spectra and photos of NEU20 and different light sources after irradiation.

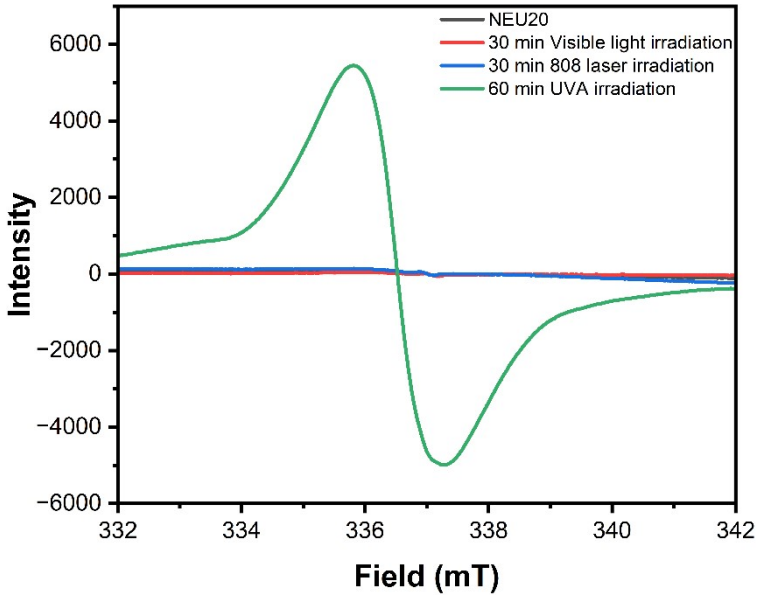

Fig. S6 EPR spectra of NEU20 and different light sources after irradiation.

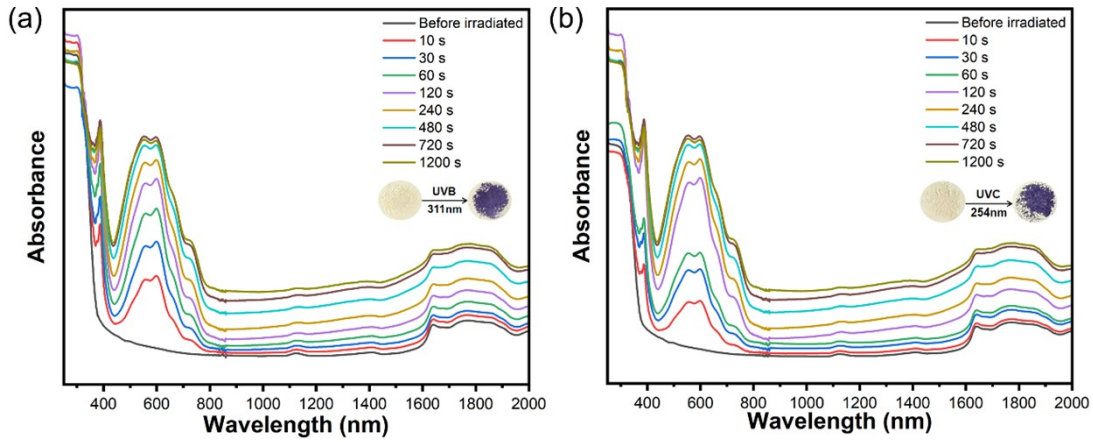

Fig. S7 *In situ* time dependent UV-Vis spectra and photographs showing the photochromic behaviors of **NEU20** by different modes of UV irradiation. (a) UVB light irradiation. (b) UVC light irradiation.

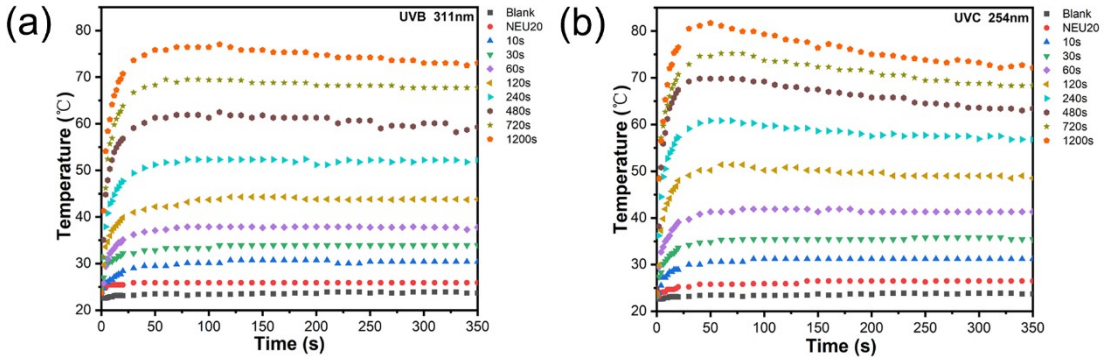

Fig. S8 Photothermal conversion curves of **NEU20-P** films on quartz glass with different modes of UV light under laser irradiation (808 nm, 1.12 W cm^{-2}). (a) UVB light irradiation. (c) UVC light irradiation.

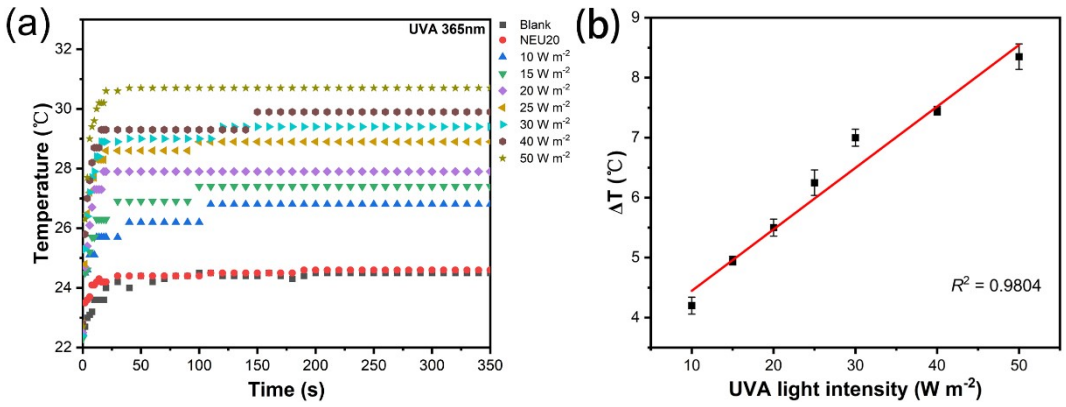

Fig. S9 (a) Photothermal conversion curves of NEU20-P films on quartz glass with different UVA light intensity under laser irradiation (808 nm, 1.12 W cm^{-2}). (b) The linear relationship between the average temperature rise (ΔT) and UV intensity.

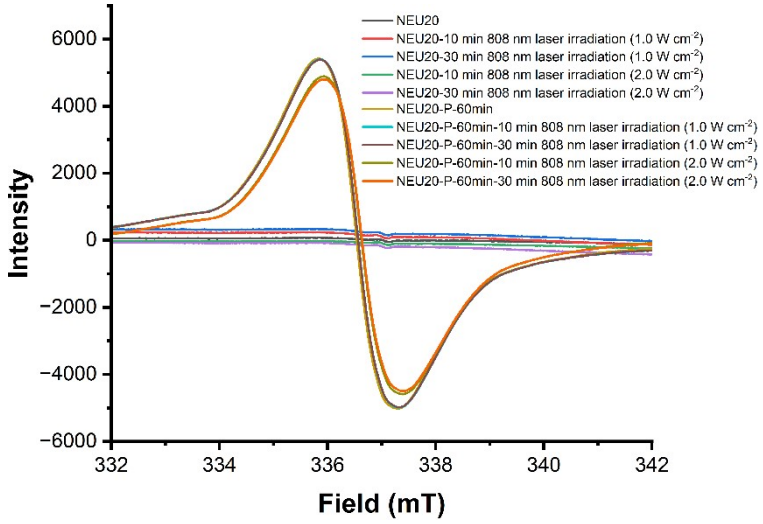

Fig. S10 EPR spectra of NEU20 and NEU20-P-60min after irradiation with different NIR laser powers.

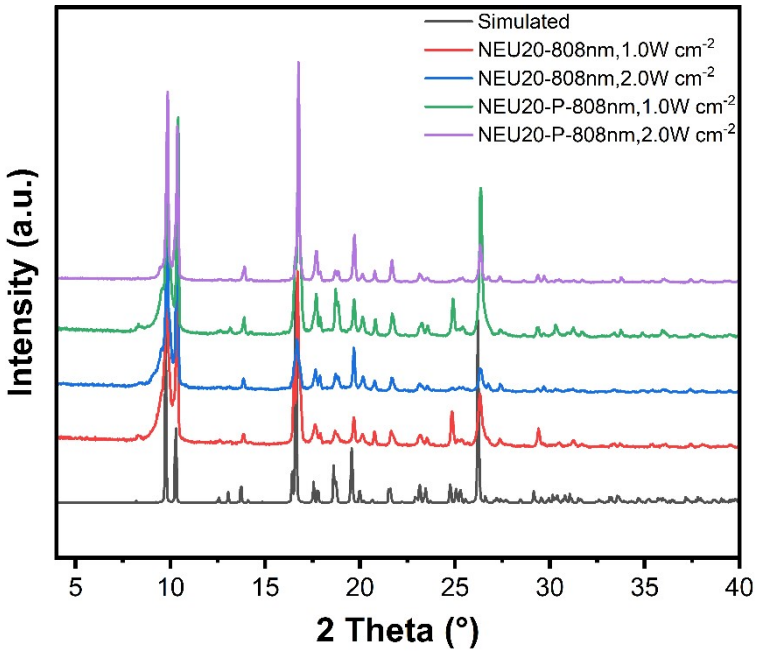

Fig. S11 PXRD for **NEU20** and other samples after 30 min of NIR laser radiation at different laser powers.

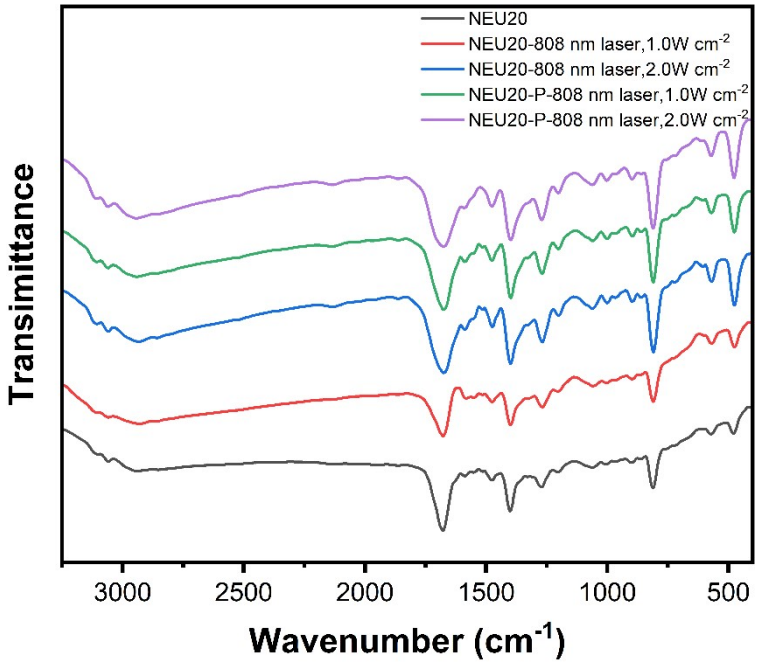

Fig. S12 IR for **NEU20** and other samples after 30 min of NIR laser radiation at different laser powers.

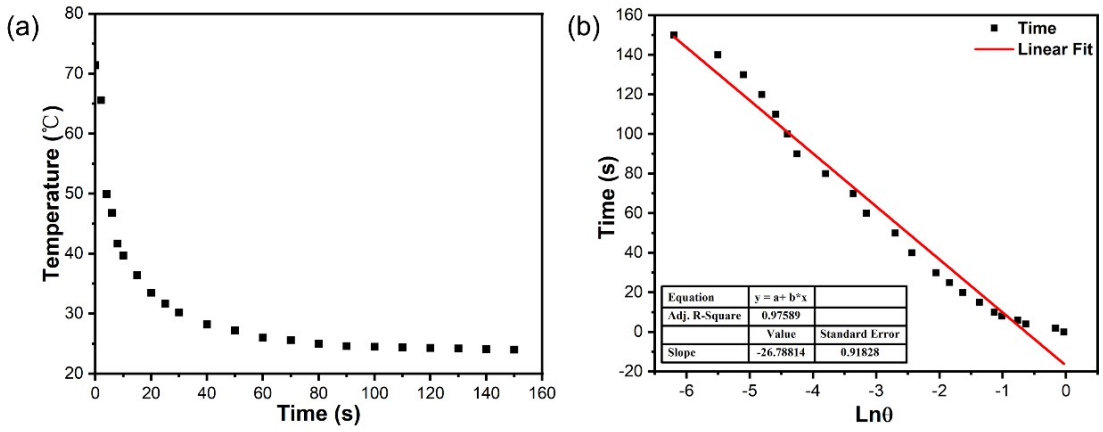

Fig. S13 (a) The cooling curve of **NEU20-P-60min** film after irradiation with 808 nm laser (1.12 $W \cdot cm^{-2}$). (b) and its corresponding time-lnθ linear curve.

2. Supplementary Table

Table S1 The photothermal properties in this work compared with previous results of solid materials in the literature.

Ref	Classif-ication	Samples	Light Source	Light Intensity	Added Temperature	Temperature Rate	η_{PT}
This work	Photo-chromic material	**NEU20**	808 nm NIR laser	1.12 W cm^{-2}	49.1 ℃ in 80 s	0.614 ℃/s	81.3 %
1		Zr-PDI MOF	808 nm NIR laser	0.7 W cm^{-2}	89 ℃ in 200 s	0.445 ℃/s	52.3 %
2		La-MV MOF (film)	808 nm NIR laser	2 W cm^{-2}	121.9 ℃ in 200 s	0.609 ℃/s	77 %
3		SOF	660 nm laser	1 W cm^{-2}	41 ℃ in 10 min	0.068 ℃/s	50.3 %
4		150-DGIST-4	808 nm NIR laser	2 W cm^{-2}	158 ℃ in 80 s	1.975 ℃/s	31.37 %
4		75-DGIST-4	808 nm NIR laser	2 W cm^{-2}	107 ℃ in 80 s	1.338℃/s	26.61 %
5		I-Rb-NDI	808 nm NIR laser	1.6 W cm^{-2}	113 ℃ in 2 min	0.942 ℃/s	23.3%
5		II-Rb-NDI	808 nm NIR laser	1.6 W cm^{-2}	141 ℃ in 2 min	1.175 ℃/s	32.1%
5		I-Cs-NDI	808 nm NIR laser	1.6 W cm^{-2}	86 ℃ in 2 min	0.717 ℃/s	31.5%
5		II-Cs-NDI	808 nm NIR laser	1.6 W cm^{-2}	145 ℃ in 2 min	1.208 ℃/s	52.6%
6	Inorganic materials	Au nanoshells	800 nm NIR laser	2 W cm^{-2}	13 ℃ in 5 min	0.043 ℃/s	13%
6		Au nanorods	800 nm NIR laser	2 W cm^{-2}	20 ℃ in 5 min	0.067 ℃/s	21%
6		$Cu_{2-x}Se$ nanocrystals	800 nm NIR laser	2 W cm^{-2}	22 ℃ in 5 min	0.073 ℃/s	22%
7		Bi_2S_3 nanorods	808 nm semiconductor laser	0.25 W cm^{-2}	22 ℃ in 300 s	0.073 ℃/s	78.1%
8		H-Pd NSs	800 nm NIR laser	1 W cm^{-2}	34.8 ℃ in 10 min	0.058 ℃/s	35.1%
9		Co_3O_4 NPs	808 nm semiconductor diode laser	1 W cm^{-2}	30 ℃ in 5 min	0.1 ℃/s	40.48 %
10		WO_{3-x} @HA	1064 nm laser	1 W cm^{-2}	38 ℃ in 10 min	0.063 ℃/s	43.6 %
11		Au-on-Au Nanorods	1060 nm laser	1 W cm^{-2}	55 ℃ in 10 min	0.092 ℃/s	67.2 %
12	Organic materials	DTC cocrystals	808 nm NIR laser	0.7 W cm^{-2}	30 ℃ in 100 s	0.3 ℃/s	18.8 %
13		Selenophene derivative polymer films	808 nm NIR laser	2.33 W cm^{-2}	30 ℃ in 3 min	0.167 ℃/s	42.5 %
14		Terrylenedi-imide-poly (acrylic acid)	660 nm laser	1 W cm^{-2}	36.8 ℃ in 10 min	0.061 ℃/s	41 %

15	Organic materials	RC-BSA NPs	915 nm laser	1 W cm^{-2}	23 ℃ in 10 min	0.038 ℃/s	28.7 %
16		Por-DPP NPs	808 nm NIR laser	1 W cm^{-2}	25.1 ℃ in 10 min	0.042 ℃/s	62.5 %
17		FA-CNPs	808 nm NIR laser	0.7 W cm^{-2}	36.4 ℃ in 5 min	0.121 ℃/s	36.5 %
18		TDI NPs	685 nm laser	0.7 W cm^{-2}	35 ℃ in 10 min	0.058 ℃/s	43.8 %
19		NBDP NPs	808 nm NIR laser	0.75 W cm^{-2}	45 ℃ in 5 min	0.15 ℃/s	54 %
20		TPP-NN NPs	638 nm laser	1 W cm^{-2}	30 ℃ in 5 min	0.1 ℃/s	36 %
21	MOF materials	TCNQ@ Ru-MOF	908 nm laser	1.262 W cm^{-2}	39.1 ℃ in 960 s	0.041 ℃/s	29 %
22		Ag-Py-2D-MOF	808 nm NIR laser	0.5 W cm^{-2}	24.5 ℃ in 3 min	0.136℃/s	22.1 %
23		Dy-2D-MOF	1 sun light	0.1 W cm^{-2}	34.7 ℃ in 4 min	0.145 ℃/s	-
24		HKUST-1	UV-Vis (300-650 nm)	0.5 W cm^{-2}	98.5 ℃ in 30 min	0.055 ℃/s	33.6 %
24		UiO-66	UV-Vis (300-650 nm)	0.5 W cm^{-2}	17.8 ℃ in 30 min	0.010 ℃/s	5.0 %
24		UiO-66-NH_2	UV-Vis (300-650 nm)	0.5 W cm^{-2}	112.5 ℃ in 30 min	0.063 ℃/s	59.3 %
24		ZIF-8	UV-Vis (300-650 nm)	0.5 W cm^{-2}	12.8 ℃ in 30 min	0.007 ℃/s	0.3 %
24		ZIF-67	UV-Vis (300-650 nm)	0.5 W cm^{-2}	100.1 ℃ in 30 min	0.056 ℃/s	50.0 %
24		CPO-27-Zn	UV-Vis (300-650 nm)	0.5 W cm^{-2}	108.2 ℃ in 30 min	0.06 ℃/s	23.8 %
24		CPO-27-Ni	UV-Vis (300-650 nm)	0.5 W cm^{-2}	139.7 ℃ in 30 min	0.078 ℃/s	93.6 %
24		CPO-27-Mg	UV-Vis (300-650 nm)	0.5 W cm^{-2}	100.5 ℃ in 30 min	0.056 ℃/s	21.6 %
24		Fe-MIL-101-NH_2	UV-Vis (300-650 nm)	0.5 W cm^{-2}	113.2 ℃ in 30 min	0.063 ℃/s	86.6 %
24		IRMOF-3	UV-Vis (300-650 nm)	0.5 W cm^{-2}	86.1 ℃ in 30 min	0.048 ℃/s	25.8 %

References

1. B. Lu, Y. Chen, P. Li, B. Wang, K. Mullen and M. Yin, Stable radical anions generated from a porous perylenediimide metal-organic framework for boosting near-infrared photothermal conversion, *Nat. Commun.*, 2019, **10**, 767.
2. S. Wang, S. Li, J. Xiong, Z. Lin, W. Wei and Y. Xu, Near-infrared photothermal conversion of stable radicals photoinduced from a viologen-based coordination polymer, *Chem. Commun.*, 2020, **56**, 7399-7402.
3. W. Z. Li, H. Chen, M. N. Shen, Z. Yang, Z. Fan, J. Xiao, J. Chen, H. Zhang, Z. Wang and X. Q. Wang, Chaotropic effect stabilized radical-containing supramolecular organic frameworks for photothermal therapy, *Small*, 2022, **18**, e2108055.
4. S. Park, J. Lee, H. Jeong, S. Bae, J. Kang, D. Moon and J. Park, Multi-stimuli-engendered

radical-anionic MOFs: Visualization of structural transformation upon radical formation, *Chem*, 2022, **8**, 1993-2010.

5. H. Ke, X.-M. Zhu, S.-M. Xie, P.-X. Ming and J.-Z. Liao, Ultrastable radicals in naphthalenediimide-based materials and their stimulus-boosting near-infrared photothermal conversion, *Inorg. Chem. Front.*, 2022, **9**, 2568-2574.
6. C. M. Hessel, V. P. Pattani, M. Rasch, M. G. Panthani, B. Koo, J. W. Tunnell and B. A. Korgel, Copper selenide nanocrystals for photothermal therapy, *Nano Lett*, 2011, **11**, 2560-2566.
7. J. Jiang, X. Che, Y. Qian, L. Wang, Y. Zhang and Z. Wang, Bismuth sulfide nanorods as efficient photothermal theragnosis agents for cancer treatment, *Frontiers in Materials*, 2020, **7**.
8. S. Li, K. Gu, H. Wang, B. Xu, H. Li, X. Shi, Z. Huang and H. Liu, Degradable holey palladium nanosheets with highly Active 1D nanoholes for synergetic phototherapy of hypoxic tumors, *J. Am. Chem. Soc.*, 2020, **142**, 5649-5656.
9. X. Huang, H. Cai, H. Zhou, T. Li, H. Jin, C. E. Evans, J. Cai and J. Pi, Cobalt oxide nanoparticle-synergized protein degradation and phototherapy for enhanced anticancer therapeutics, *Acta Biomater*, 2021, **121**, 605-620.
10. Y. Ding, R. Huang, L. Luo, W. Guo, C. Zhu and X.-C. Shen, Full-spectrum responsive WO_{3-x}@HA nanotheranostics for NIR-II photoacoustic imaging-guided PTT/PDT/CDT synergistic therapy, *Inorg. Chem. Front.*, 2021, **8**, 636-646.
11. J. Jia, G. Liu, W. Xu, X. Tian, S. Li, F. Han, Y. Feng, X. Dong and H. Chen, Fine-tuning the homometallic interface of Au-on-Au nanorods and their photothermal therapy in the NIR-II window, *Angew. Chem., Int. Ed.*, 2020, **59**, 14443-14448.
12. Y. Wang, W. Zhu, W. Du, X. Liu, X. Zhang, H. Dong and W. Hu, Cocrystals strategy towards materials for near-infrared photothermal conversion and imaging, *Angew. Chem., Int. Ed.*, 2018, **57**, 3963-3967.
13. B. Kim, H. Shin, T. Park, H. Lim and E. Kim, NIR-sensitive poly(3,4-ethylenedioxyselenophene) derivatives for transparent photo-thermo-electric converters, *Adv. Mater.*, 2013, **25**, 5483-5489.
14. S. Zhang, W. Guo, J. Wei, C. Li, X. J. Liang and M. Yin, Terrylenediimide-based intrinsic theranostic nanomedicines with high photothermal conversion efficiency for photoacoustic imaging-guided cancer therapy, *ACS Nano*, 2017, **11**, 3797-3805.
15. B. Zhou, Y. Li, G. Niu, M. Lan, Q. Jia and Q. Liang, Near-infrared organic dye-based nanoagent for the photothermal therapy of cancer, *ACS Appl. Mater. Interfaces*, 2016, **8**, 29899-29905.
16. F. Wu, L. Chen, L. Yue, K. Wang, K. Cheng, J. Chen, X. Luo and T. Zhang, Small-molecule porphyrin-based organic nanoparticles with remarkable photothermal conversion efficiency for in vivo photoacoustic imaging and photothermal therapy, *ACS Appl. Mater. Interfaces*, 2019, **11**, 21408-21416.
17. Z. He, L. Zhao, Q. Zhang, M. Chang, C. Li, H. Zhang, Y. Lu and Y. Chen, An acceptor–donor–acceptor structured small molecule for effective NIR triggered dual phototherapy of cancer, *Adv. Funct. Mater.*, 2020, **30**, 1910301.
18. T. Sun, H. Liu, N. Jiang, Q. Wu, C. Li, R. Xia, B. Gao and Z. Xie, Unadulterated organic nanoparticles with small sizes for robust tumor imaging and photothermal treatment, *Adv. Funct. Mater.*, 2021, **31**, 2103714.
19. N. Song, Y. Li, L. Chen, X. Hu and Z. Xie, Bodipy derivatives as light-induced free radical

generators for hypoxic cancer treatment, *J. Mater. Chem. B*, 2019, **7**, 3976-3981.

20. R. Xia, X. Zheng, X. Hu, S. Liu and Z. Xie, Photothermal-controlled generation of alkyl radical from organic nanoparticles for tumor treatment, *ACS Appl. Mater. Interfaces*, 2019, **11**, 5782-5790.
21. T. Zhang, J.-W. Cao, X. Jiang, J. Chen, T. Wang and K.-J. Chen, Band gap modulation enabled by TCNQ loading in a Ru-based metal–organic framework for enhanced near-infrared absorption and photothermal conversion, *Crystal Growth Des.*, 2021, **21**, 729-734.
22. M. Q. Li, M. Zhao, L. Y. Bi, Y. Q. Hu, G. Gou, J. Li and Y. Z. Zheng, Two-dimensional silver(I)-dithiocarboxylate coordination polymer exhibiting strong near-infrared photothermal effect, *Inorg. Chem.*, 2019, **58**, 6601-6608.
23. J. Su, N. Xu, R. Murase, Z. M. Yang, D. M. D'Alessandro, J. L. Zuo and J. Zhu, Persistent radical tetrathiafulvalene-based 2D metal-organic frameworks and their application in efficient photothermal conversion, *Angew. Chem., Int. Ed.*, 2021, **60**, 4789-4795.
24. J. Espin, L. Garzon-Tovar, A. Carne-Sanchez, I. Imaz and D. Maspoch, Photothermal activation of metal-organic frameworks using a UV-Vis light source, *ACS Appl. Mater. Interfaces*, 2018, **10**, 9555-9562.